Journal of Materials Chemistry A

Accepted Manuscript

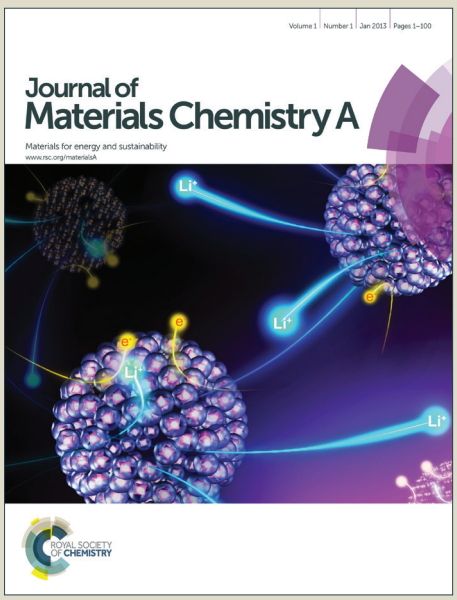

ROYAL SOCIETY OF CHEMISTRY

www.rsc.org/materialsA

Doped h-BN monolayer as efficient noble metal-free catalysts for CO oxidation: role of dopant and water in activity and catalytic de-poisoning

S. Sinthika, E. Mathan Kumar and Ranjit Thapa*

SRM Research Institute, SRM University, Kattankulathur - 603203, Tamil Nadu, India

ABSTRACT

Using first principles approach, we investigate the catalytic activity of noble metal-free n-doped (C→B, O→N) hexagonal boron nitride (h-BN) monolayer for CO oxidation. To be mentioned CO adsorption ability, and hence the preferred Eiley-Rideal (ER) and Langmuir Hinshelwood (LH) mechanism for CO oxidation is dopant-dependent: CO is chemisorbed on O-doped h-BN (OBN) while it interacts physically with C-doped h-BN (CBN) surface. Even though both C and O doping create similar donor states below the Fermi level (E_f), the O doping results in larger bond length of O-B1 (one of the nearest B atom), out-of plane displacement of B1 atom and less positive charge on B1 atom, synergistically making this atom higher in activity. The presence of a pre-adsorbed O_2 molecule in both types of surfaces eliminates any chances of CO poisoning of the surface and CO oxidation prefers to proceed via ER mechanism with small activation barrier. *The high values of Sabatier activities suggest doped h-BN surface to be superior to Au_{55} and Pt_{55} nanoclusters.* In case of CO oxidation by means of LH mechanism, a stable O_2···CO intermediate is produced, which requires quite high barrier energy to break the O-O bond. However, the presence of a H_2O molecule increases the activity of the catalyst and helps in catalytic CO de-poisoning.

*Corresponding Author E-mail: ranjit.t@res.srmuniv.ac.in, Tel. No.: +91-44-27417918, Fax: +91-44-27456702

Keywords: Catalyst, Adsorption, Sabatier activity, Activation energy, DFT.

1 Introduction

The design and development of novel metal-free catalysts have made rapid progress in the recent years,[1-3] with increasing concerns over the limited abundance and high cost of conventional precious-metal based catalysts[4]. For instance, platinum which is widely used in the design of catalytic converters in automobiles for the oxidation of incomplete combustion products like CO, hydrocarbons and NO_x, is highly expensive. In addition to this, platinum based materials, when used as fuel-cell electrocatalysts are susceptible to time-dependent drift and are highly sensitive to CO impurities, thereby hindering the lifetime and efficiency of such catalysts.[5,6] On the contrary, catalysts based on nanoparticles, especially unsupported nanoporous gold are more tolerant to CO poisoning and have proven to be efficient electrocatalysts even at low temperatures.[7] Moreover, the presence of water molecules also aid in enhancing the catalytic activity of Au nanoparticles.[8] But catalysts that are entirely noble metal-free[9] are in great demand as they are inexpensive and environment friendly, making them suitable candidates for green chemistry.[10]

Theoretical studies on noble metal-free catalysts like nitrogen doped carbon nanotubes[10,11] doped graphene[12-14] and metal doped boron nitride,[15,16] have inferred that heteroatom doping modifies the electronic properties (by introducing defect states near the Fermi level), enhances charge transfer from the surface to the reactant and/or induces bond polarization due to electronegativity difference between the dopant and a neighboring site, making the host materials highly active for the catalytic conversion of CO to CO_2. Also to design a good catalyst for CO oxidation, an atomic-level understanding of the adsorption energies, reaction intermediates, barrier energies and reaction energies are very essential.[15] Generally, CO oxidation is known to proceed according to the proposed mechanisms: the Langmuir–Hinshelwood (LH) mechanism and Eley–Rideal (ER) mechanism. The LH

mechanism involves the adsorption of both CO and O_2 on the available active sites, followed by a surface reaction, while in the ER mechanism an approaching CO molecule directly reacts with an adsorbed O_2 molecule.[17] Trends in the catalytic activity of materials can be identified based on the Sabatier principle:[18] the adsorption energies of the reactants should neither be too strong nor too weak. Also, the activation energies of the rate determining steps (RDS) in a catalytic reaction play a vital role in determining the activity: the lower the activation energy, the higher the reaction rate.[19] Density functional theory (DFT) can be used to qualitatively describe the catalytic reactions on various surfaces considering all the above understanding and hence the detail of various steps and mechanism is necessary for designing a new class of catalyst.[20]

Hexagonal boron nitride (h-BN) has recently attracted the interest of many researchers because of its unique properties including high thermal conductivity and high thermal stability that distinguishes it from its much-studied analogous counterpart, graphene. Though pristine h-BN is considered to be a highly inert insulator, modifying its electronic structure can remarkably affect its adsorption properties, and hence enhance its catalytic activity. For instance, it has been theoretically observed that h-BN monolayer supported on Ni (111) is an efficient catalyst for CO oxidation and the process takes place selectively via the ER mechanism.[21] Doping h-BN with metals has also proven to be efficient in the catalytic conversion of CO to CO_2 as elucidated by Lin et al.[15]

In this work, we investigate the catalytic activity of electron (n) doped h-BN monolayer during CO oxidation. Carbon and oxygen have been employed as dopants and we computationally investigate the dopant-dependent mechanism by which CO oxidation occurs. The ER and LH mechanisms are investigated in detail and we find that the ER mechanism occurs with small activation barriers for both the cases. LH mechanism was also investigated

and it is found that in oxygen doped h-BN, a O_2···CO intermediate is produced and the energy barrier for the RDS, i.e to form first CO_2 is high (1.5 eV). But in the presence of water molecule, the barrier is notably reduced to 1.22 eV, which suggests that water plays a significant role to increase the activity of catalyst.

2 Computational Details

Theoretical calculations were performed using spin polarized density functional theory as implemented in the CASTEP code.[22] Ultrasoft pseudopotentials were used to describe the core electrons.[23] The Perdew, Burke and Ernzerhof (PBE)[24] generalized gradient approximation (GGA) was employed for describing the exchange-correlation potentials. For long-range van der Waals interaction, the parameter-free Tkatchenko−Scheffler method was used to correct the PBE total energy.[25] Henceforth this approach is termed as PBE+D. Brillouin zone sampling was made with the Monkhorst Pack scheme and a K-Point grid of 5x5x1. It was found that cut-off energy of 400 eV is sufficient to give well-converged results. All the structures were optimized until the total energy converged to less than 10^{-5}eV/atom and the maximum force converged to lower than 0.01 eV/Å. In order to cross check the results with PAW potentials, the Vienna Ab initio Simulation Package (VASP) was also employed.[26,27] The linear and quadratic synchronous transit method (LST/QST) implemented in CASTEP was used to search for Transition states.[28] The nudged elastic band (NEB) method was also employed to validate results of transition states.

The adsorption energy of the reactants on the surface was calculated as the difference between the total energy of the molecule and surface when they are far apart (~10Å) and the total energy of the molecule adsorbed on the surface.

The reaction energy is defined as the difference between the energies of two successive steps in the reaction pathway. The change in free energy ($\Delta G=\Delta E-T\Delta S$) is defined as the difference in free energies between two successive steps in the reaction pathway.

3 Results and Discussions

3.1 Structural Analysis

The effects of carbon and oxygen doping on h-BNs were investigated for the following cases (i) replacement of a boron atom with a carbon atom (CBN) (ii) an oxygen atom replacing a nitrogen atom (OBN). These two cases can be considered as models of one electron doping of the h-BN sheet. Since the formation energy of an oxygen atom replacing a boron atom of h-BN is very high, this structure is predicted to be highly unstable,[29] and hence we did not investigate this case. From the optimized structures (shown in Fig. 1a), it has been found that the atoms in CBN surface lie in the plane and do not move outward after relaxation. The C-N bond lengths are 1.40 Å, which is only 0.04 Å shorter than the C-N bond of pristine h-BN. The C dopant in CBN carries a Mulliken charge of +0.34 e. In OBN, a boron atom (denoted as B1) adjacent to the oxygen dopant is displaced downward by 0.5 Å from the plane. The nearest boron atom distances from the oxygen dopant are O-B1 = 1.60Å, O-B2 = 1.44 Å and O-B3 = 1.44 Å, showing that the O-B1 bond length is higher than the other O-B bonds by 11.1%. Mulliken charge analysis reveal that the O dopant in OBN imparts unequal amounts of charge to the surrounding boron atoms, with B1 = +0.53 e, B2 = +0.93 e and B2 = +0.93 e. The structural modification (higher O-B1 bond length) and the less positive Mulliken charge on B1 atom due to O-doping indicate the higher activity of particular B atom with respect to other B atoms. This is quite similar to the case of phosphorous doped graphene, wherein the displacement of phosphorous atom from the graphitic plane results in increased surface reactivity of the plane.[30]

3.2 Constrained potential energy curve

Before investigating the mechanism of CO oxidation on the surfaces, the adsorption of the reactants, CO and O_2 were studied systematically in order to test for CO tolerance. It is

well known by now that pristine h-BN sheets are highly inactive and hence do not adsorb any reactant molecules.[21] Addition of the n-type dopant C makes the h-BN structure reactive and O_2 is adsorbed rather strongly in the B atom nearest to the C dopant with an adsorption energy of E_{ad} = -1.77 eV. The adsorbate-surface distance is about 1.58 Å and the molecular bond length of oxygen is increased to about 1.34 Å, (free O_2 molecule in triplet state the bond length is 1.24 Å) indicating that the oxygen molecule is highly activated due to the electronic charge transfer from the BN sheet to the $2\pi^*$ orbital of O_2. Increasing the number of C dopants to two (two-electron doping, henceforth denoted as 2CBN) results in a much stronger adsorption of the O_2 molecule, with the O_2 molecule being adsorbed in the side-on form. The molecular bond length of O_2 is elongated to 1.53 Å, and the distance from the surface is 1.48 Å, with E_{ad} = -3.93 eV, indicating a much stronger chemisorption.[31] The OBN surface adsorbs the oxygen molecule more strongly at the displaced boron site with the adsorbate-surface distance being 1.54 Å, E_{ad} = -2.92 eV and the molecular bond length increasing to 1.34 Å. Thus, this surface may also prove to be a potent candidate for anchoring O_2, which is essential in many important catalytic reactions. The bond lengths, adsorbate-surface distances, adsorption energies and the Mulliken charges on the adsorption site after O_2 adsorption are summarized in Table 1.

Next, the adsorption of CO molecule on each of the surfaces is analyzed in detail as shown in Fig. 1. We systematically examined the several possible adsorption sites in order to find the most preferred site for CO adsorption. It was found that CO prefers to adsorb with the C atom facing the active site. Interestingly, the adsorption behavior of CO molecule is different for CBN and OBN, even though the two systems can be considered as typical cases of one-electron doping. For a thorough analysis of the adsorption behavior of CO on the catalytic surfaces, constrained potential energy (PE) curves[32] were constructed keeping the distance between the approaching CO molecule and active atom on CBN surface fixed and

relaxing the entire system and the curves are shown in Fig. 1b and 1c**.** Two possible sites (B and C) were tested for CO adsorption. Since the adsorption of CO on most surfaces is found to be in the physisorbed range, van der Waal's corrected final energy was also used to plot the potential energy curves. The CO molecule adsorbs rather weakly on a B (Fig. 1b), with the potential energy curve showing two dips, signifying that the van der Waals dispersion effect becomes more pronounced at larger distances, with the dip at the CO - CBN distance of about 3.31 Å being deeper than that calculated using PBE alone. The binding energies for nearer distance are E_{ad} = +0.344 eV/-0.035 eV (PBE/PBE+D), and for far distance E_{ad}= -0.024 eV/-0.14 eV (PBE/PBE+D). The estimated value of binding energies indicates formation of very weak physical bond of CO molecule with the surface atoms. On the C site (see Fig. 1c), there is a modest increase in the surface-adsorbate interaction, with E_{ad} = -0.024 eV/-0.14 eV (PBE/PBE+D), suggesting that the dopant carbon site is more favourable for CO molecular adsorption.

The constrained PE curves of approaching CO molecule on 2CBN surface are shown in Fig. 1d and 1e.The adsorption energy of CO molecule is higher on 2CBN surface than the CBN system. On the B site as shown in Fig. 1d, for the lowest PE, the CO-surface distance is ~1.72 Å with E_{ad} =-0.08 eV/-0.24 eV (PBE/PBE+D) and for the C site of 2CBN shown in Fig. 1e, CO adsorbs at ~ 1.69 Å from the surface with E_{ad} = -0.15 eV/-0.31 eV (PBE/PBE+D), suggesting that the C site is more favorable for CO adsorption. The adsorption of CO is highly favorable on OBN surface. The CO molecule prefers the B site adjacent to the O dopant, and the constrained PE curve is shown in Fig. 1f. The CO molecule is chemisorbed on B site with E_{ad} = -1.33 eV/-1.44 eV (PBE/PBE+D). The C atom of CO molecule is facing the boron atom and the bond length (C-O) increases to 1.20Å (the bond length of CO in the gas phase is 1.15 Å). Because of the chemisorption of CO molecule, the PBE and PBE+D potential energy curves are quite similar. This adsorption of CO results in

the competition of both ER and LH mechanisms on active boron sites, and will be discussed in detail in the later section. In the point of view of adsorption energies, CO adsorption is energetically less favorable than O_2 adsorption for both the cases of doping, which is a desirable criterion while designing a good catalyst for CO oxidation.[14] The details of CO adsorption in the chosen sites of the different surfaces are tabulated in Table 2.

3.3 Role of dopant: Partial density of states

In order to gain a deeper insight into the adsorption behaviour of CO on the doped surfaces, the electronic structures of these systems are studied. The spin polarized partial density of states (PDOS) of the C and B doped h-BN are shown in Fig. 2. Fig. 2a & 2d demonstrate the PDOS of CO-CBN and CO-OBN respectively wherein the CO molecule is considered to be sufficiently far (~ 6 Å) from the surface. The extra donor electronic state below the Fermi level of the surfaces of CBN and OBN is a clear indication of one– electron doping of the hBN sheet. It can also be observed that the $2\pi^*$ orbital of free CO is empty and lies above the Fermi level. Fig. 2b shows the PDOS of CO adsorbing on the B site of CBN surface. The PDOS shows no strong hybridization between the CO molecule and the p states of CBN, indicating that CO does not interact too strongly with the B site of CBN. From the PDOS for the CO adsorbed on C site of CBN in Fig. 2c, it is clear that there is electron donation from the surface to the $2\pi^*$ orbital of the CO molecule, making it partially occupied. In the case of CO adsorbed on OBN Fig. 2e, there is larger amount of charge transfer from the surface p states to the CO $2\pi^*$ orbital, resulting in a stronger adsorption in comparison to the C doped h-BN sheet. Fig. 2f shows the PDOS of the oxygen dopant atom and the active boron site (B1) (see Fig. 1a) of OBN, which indicate that the extra electron for charge transfer is provided by the active boron site (as discussed in the earlier section, this particular

B atom has less positive charge compare to other B atom), while in the case of CBN, (Fig. 2c), the carbon dopant itself acts as the donor of electrons.

3.4 Co-adsorption

We further analysed the co-adsorption of O_2 and CO by investigating how the presence of one pre-adsorbed reactant affects the other. The nature of co-adsorption of O_2 and CO will determine the mechanism by which CO oxidation occurs on the surface. Fig. 3a shows the dioxygen adsorbed CBN surface, wherein the CO molecule was placed on the top of carbon site (near to the surface) before relaxation. From the relaxed structure it was found that, the presence of O_2 greatly hinders the adsorption of CO, which results in physisorption of CO at 3.28 Å from the surface. This may be due to the fact that the strong chemisorption of pre-adsorbed O_2 to the surface results in an almost complete one electron transfer from the surface states to O_2, leaving behind no electrons to partcipate in bonding with CO (DOS shown in Fig. S1 of the supplementary information (SI)**.** This property of the CBN surface makes it a prospective candidate in the design of highly CO tolerant catalysts which selectively adsorb O_2 molecules when a mixture of O_2/CO gas is present.[14]

Since the OBN surface anchors both CO and O_2, two cases of co-adsorption were investigated. Fig. 3b shows the adsorption of CO on the surface, pre-adsorbed with O_2. The results are almost similar to those obtained in the case of CBN, with the CO-surface distance being 3.04 Å and the adsorption energy in the physisorbed range. The PDOS of O_2, CO and the surface is shown in Fig. 3d, from which it is evident that there is an electron transfer from the donor level of the surface to one of the $2\pi^*$ states of O_2, while the CO molecular levels are almost unaffected. Fig. 3c shows the relaxed structure of O_2 adsorption on OBN, pre-adsorbed with CO. The O_2 is also bound to the surface at a distance of 2.69Å and E_{ad} = -1.73 eV. Since O_2 exhibits stronger ability as electron-acceptor molecule than the CO molecule,[4]

the charge transfer from the surface to CO is incomplete and we expect some amount of charge transfer from the surface to the approaching O_2 as is apparent from the PDOS in Fig. 3e, which shows that the molecular levels of both CO and O_2 are broadened due to the interaction with the surface. It can also be seen that the co-adsorption of CO and O_2 in OBN results in the formation of a bond (OC···OO = 1.53 Å) between the reactant molecules, paving way for the LH mechanism to take place. From a charge density difference plot of this intermediate (see Fig. S3 of SI), it can be seen that there is high electron accumulation on the B-C (substrate-molecule) bond, confirming that the intermediate is chemisorbed to the surface. The CO-O_2 bond also shows regions of electron accumulation, demonstrating that this bond is rather strong.

3.5 Free energy profile and CO oxidation mechanism

Next, the mechanism of CO oxidation is investigated in detail. Free energy change (ΔG) is calculated as $\Delta G = \Delta E - T\Delta S$, where ΔE is the total energy change obtained from DFT calculations, ΔS denotes the entropy change and the zero point energies (ZPE) are regarded to be negligible. We also assume the entropies of the adsorbed state to be negligible and ΔS of the gases are obtained from ref 33.Now we discuss in detail the free energy profile of two different reaction mechanisms during CO oxidation**.** The ER mechanism of CO oxidation on CBN surface is discussed first. The resultant free energy profile with reaction steps is shown in Fig. 4a and the corresponding relaxed atomic configurations at each step along the reaction pathway are shown in Fig. S2 of SI. The initial step is taken to be the one in which 2CO molecules, an O_2 molecule and the surface are sufficiently far from each other without any interaction. The next step involves the adsorption of O_2 to the surface which is exothermic. In step 3, a CO molecule is made to react with this adsorbed O_2. It was found that if the CO molecule was placed close enough to O_2, after geometry optimization, the O−O bond is broken to form CO_2 with atomic O remaining adsorbed to surface. If the CO-O_2 distance was

made larger than a certain distance, the CO molecule moves away from O_2 after relaxation. This indicates that the formation of O_2···CO type intermediate is unfavorable and even if it forms, it will be unstable and CO_2 desorption is fast. This makes the accurate calculation of the activation barrier difficult. A similar phenomenon was also observed by Wasey et al.[21] on a h-BN monolayer on Ni (111) surface, where they have stated that the reaction takes place spontaneously without any activation barrier. In order to calculate the small activation barrier, we constructed constrained potential energy curves keeping the CO – O_2 distance fixed and relaxing the entire system. The structure shown in the right inset of Fig. 4a represents the configuration chosen, with the reaction coordinate (Z) taken as the distance between the adsorbed O_2 and the approaching CO. The resulting potential energy curve plot is shown in the left inset of Fig. 4a, from which it can be inferred that the activation energy (E_a) is indeed small and is equal to 0.26 eV. This step can be considered as the RDS. The reaction energy for the conversion of first CO to CO_2 is calculated to be -2.9 eV. The interaction of the next CO molecule with the highly reactive atomic oxygen and the subsequent formation of CO_2 (step 4) take place with a small barrier, with a reaction free energy of -2.35 eV. In OBN, the results are similar, with the activation energy barrier for the formation of first CO_2 being equal to 0.16 eV and the formation of next CO_2 takes place with a rather small barrier, with ΔG = -0.73 eV. The schematic energy profile is shown in Fig. 4b. As discussed earlier, CO molecule doesn't adsorb on CBN surface in presence of O_2 molecule, indicating that the LH mechanism is less favorable in this particular structure.

Now we discuss about CO oxidation following LH mechanism at OBN surface (shown in Fig. 4c), since the probability of adsorption of both the reactants is high at this surface. Recalling that the presence of pre-adsorbed O_2 strongly repels CO adsorption, we consider the case wherein the CO molecule is adsorbed first and an O_2 is adsorbed in a neighbouring site. The initial step in the reaction pathway is taken to be the non-interacting

2CO, O_2 and the surface. The first step involves the co-adsorption of both reactants, which results in the formation of O_2···CO complex intermediate and is exothermic. This is followed by desorption of the first CO_2 from the catalyst surface, which can be considered as the RDS, requiring an E_a of 1.55 eV (the initial and final structure are shown in Fig. 4d(I)). The next step involves the interaction of the remaining O atom and the second CO molecule to form CO_2. This reaction is found to be endothermic when the reaction energies are considered as such (+0.16 eV), but is exothermic (ΔG = -0.49 eV) when the entropic energy term, $T\Delta S$, was considered along with the total energy (see Fig. 4c).

Having calculated the activation barriers for the catalysts, it can be concluded that the ER mechanism is more favourable in both the catalysts and the LH mechanism may take place at high temperatures in OBN. A detailed review on previous works of CO and O_2 binding with catalyst, activation energy and preferred mechanism (ER and LH) on non-metal and metal based catalyst have been summarized in Table 3. With a view to test the effectiveness of our catalysts, we calculated the Sabatier activity (SA) of OBN following LH mechanism (see SI for calculation details) and compared it with two well-known noble metal catalysts : Au_{55} and Pt_{55} clusters. These cuboctahedral clusters are recognized as one of the stable clusters having a bulk fcc structure and they have also been synthesized experimentally.[44] There is theoretical evidence that these clusters provide active sites for the chemisorptions of both CO and O_2 suggesting that the mechanism of CO oxidation is preferably LH.[45] Our calculations reveal that in Au_{55}, O_2 adsorbs with E_{ad} = -0.49 eV and the adsorption energy of CO is -0.77 eV. (The site – dependence of the adsorption of reactants was not considered here for simplicity). O_2 dissociation is hindered by a high barrier (~ 2.48 eV) on the active sites of Au_{55}, demonstrating that it occurs only at high temperatures. There is a possibility of the formation of a stable intermediate O_2···CO and subsequent desorption of the first CO_2 occurs with barrier energy (E_a) of 0.76 eV, this step is the RDS (see Fig.

4d(II)) (also see Fig S4 for the local configurations of the reactants on the Au_{55} clusters until the desorption of first CO). In Pt_{55}, the possibility of formation of a stable intermediate is very low: the O_2 molecular chemisorption is very high with E_{ad} = -1.79 eV and CO adsorbs with E_{ad} = -1.51 eV The barrier for intermediate formation and subsequent desorption of CO_2 is very high (2.76 eV) as shown in Fig. 4d (III), proving that it does not take place at low temperatures. The barrier for O_2 dissociation is comparatively smaller (E_a = 0.60 eV), and this can be regarded as the RDS (shown in Fig. 4d (IV)), with the CO molecule reacting with an atomic oxygen to form CO_2 being the next step (E_a = 0.34 eV) (see Fig. S4, demonstrating clearly the minimum path for the CO oxidation in Pt_{55} cluster as catalyst). These results are consistent with previous work.[45] It can be observed that in only higher temperature the CO oxidation on Pt_{55} via LH mechanism follow similar path as in Au_{55}.

3.6 Sabatier Activity

Making use of the calculated E_a of the RDS of each catalyst, we calculated the Sabatier activity for ER and LH mechanisms independently (the detail calculation steps are written in the SI). Since CO oxidation in Pt_{55} takes place via dissociative chemisorption of O_2, we followed the procedure outlined in ref 46 for calculating the SA. The results indicate that the SA of CO oxidation following the ER mechanism in CBN and OBN surface is high, being, 1.31 and 1.21 respectively again proving these catalysts to be efficient for CO oxidation if the reaction proceeds via the ER mechanism. Even though the high E_a of the LH mechanism of OBN indicates that it does not take place favorably at room temperatures, we calculated the SA of this reaction, to test the activity if at all this reaction proceeds. Our calculations indicate that the SA is -0.61, which is lower than the SA of Pt_{55} (-0.24) which in turn is notably lower than that of Au_{55} (0.48). The trends in the SA are an evidence of the fact that although extended Pt surfaces show good catalytic activity and are considered to be the best catalysts for CO oxidation, small clusters of Au remarkably outperform Pt clusters in

their activity.[47] In addition, the presence of a water molecule increases the Sabatier activity of OBN surface following LH mechanism to -0.28. The details of calculation of activation energies and adsorption energies used for determining the SA is discussed in the next paragraph.

3.7 Role of water molecule

The presence of water molecules in the vicinity of a catalytic surface may invariably affect the oxidation of CO to CO_2. For instance, it has been observed by Bongiorno et al[8] that water enhances the catalytic activity of gas-phase and supported gold nanoclusters toward CO oxidation by notably reducing the activation barrier for CO_2 formation. We examine the influence of co-adsorbed water on the catalytic activity by considering the LH mechanism of OBN, since the activation barrier for the desorption of CO_2 from O_2···CO intermediate is found to be rather high in this system. The reaction pathway is illustrated in Fig. 5a.

Our calculations reveal that the adsorption of a water molecule on the OBN surface is fairly weak with E_{ad} = -0.25 eV. But, investigation of the co-adsorption of H_2O and O_2 discloses the beneficial role played by H_2O in enhancing the activity. It was noted that when a water molecule was placed at a neighbouring site of adsorbed O_2, the former acts as an attractor for O_2. The O_2 bond length is elongated more (1.35 Å) and the O-H bond of the H_2O molecule pointing toward the nearest oxygen atom of the O_2 increases to 0.98 Å. The distance between the hydrogen atom of H_2O and nearest oxygen atom of O_2 is 2.07 Å. When H_2O was co-adsorbed with both O_2 and CO (the two reactants in O_2···CO intermediate form), it was found that the energy barrier required to desorb CO_2 from the intermediate state is considerably reduced to 1.22eV. Fig. 5b depicts the relaxed structure of initial state (I.S.) of RDS, wherein a H_2O molecule interacts with O_2···CO. The presence of H_2O alters the O_2···CO intermediate, with the distance between the O_2 and surface decreasing from 2.69 Å

to 2.52Å and the distance between O_2 and CO decreasing by 0.01Å. Mulliken charge analysis reveals that there is charge transfer from a proton of H_2O to the nearest O atom of the intermediate. This in turn results in a stronger tendency of O_2 to react with the adsorbed CO making CO_2 desorption easier, as shown in the relaxed final state (F.S.) in Fig. 5c. This F.S. is found to be endothermic when the reaction energies are considered as such (+0.33 eV), but is exothermic by -0.31 eV, when the difference in free energy is considered (see Fig. 5a). The calculated results clearly indicate that the CO de-poisoning of catalyst in presence of water molecule is feasible.

In order to test the effectiveness of the catalyst in practical applications, we modeled the CBN surface on a few layers of graphite substrate and assessed its CO oxidation ability. We found that the results obtained do not vary and the properties of the catalytic surface are preserved even in the presence of the substrate (see Fig. S5 of SI).

4 Conclusions

C and O doped h-BN monolayer prefer either ER or LH mechanism for CO oxidation depending on the adsorption behavior of CO molecule. Particularly in case of C doped h-BN surface the CO molecule has very less interaction with the surface atoms, proving that the CBN surface is more tolerant to CO poisoning, and CO oxidation favours ER mechanism. In OBN, the possibility of CO chemisorptions is high, indicating both ER and LH mechanism are possible in this case. The presence of pre-adsorbed O_2 hinders the CO interaction with the active sites (in both type of surface) i.e. CO poisoning is less. But in case of pre-adsorbed CO molecule on OBN surface and subsequent approaching of O_2 molecule during CO oxidation leads to a very stable intermediate (O_2···CO) with high value of activation energy. But the presence of H_2O molecule can facilitate the de-poisoning and activity of the catalytic surface, as explained in this work considering the CO oxidation following LH mechanism. The

activity of CO oxidation in CBN and OBN surface is higher than Au_{55} and Pt_{55} nanoclusters. The DFT approach to find the activation barrier for ER mechanism in this work will provide a new mode to describe the reaction mechanism, activity and de-poisoning during CO oxidation. Overall it can be concluded that n-doped h-BN could be a suitable candidate to replace the present precious-metal based catalysts for CO oxidation.

Supplementary Information

Calculation step used in this work to find Sabatier activity during ER and LH mechanism for various catalysts. Possible reaction steps during CO oxidation on Au_{55} and Pt_{55} as catalyst.

Acknowledgements

RT thanks Science and Engineering Research Board (SERB) for the financial support (Grant no: SB/FTP/PS028/2013). All authors thank SRM Research Institute, SRM University for providing supercomputing facility and financial support. RT thanks Centre for Development of Advanced Computing (CDAC) for the supercomputing facility at Pune, India.

References

1 K. Gong, F. Du, Z. Xia, M. Durstock and L. Dai, *Science*, 2009, **323**, 760-764.

2 S. Kattel, B. Kiefer and P. Atanassov, *J. Mater. Chem. A*, 2014, DOI: 10.1039/C4TA01460J.

3 H. Wang, B. A. Kakade, T. Tamaki and T. Yamaguchi, *J. Power Sources*, 2014, **260**, 338–348.

4 D. Tang and C. Hu, *J. Phys. Chem. Lett.,* 2011, **2**, 2972–2977.

5 L. Qu, Y. Liu, J.-B. Baek and L. Dai, *ACS Nano*, 2010, **4**, 1321-1326.

6 J. P. Collman, N. K. Devaraj, R. A. Decréau, Y. Yang, Y.-L. Yan, W. Ebina, T. A. Eberspache and C. E. D. Chidsey, *Science*, 2007, **16**, 1565-1567.

7 C. Xu, J. Su, X. Xu, P. Liu, H. Zhao, F. Tian and Y. Ding, *J. Am. Chem. Soc.*, 2007, **129**, 42–43.

8 A. Bongiorno and U. Landman, *Phys. Rev. Lett.*, 2005, **95**, 106102.

9 R. Cao, R. Thapa, H. Kim, X. Xu, M. G. Kim, Q. Li, N. Park, M. Liu and J. Cho, *Nature Commun.*, 2013, **4**, Article No. 2076.

10 X. Hu, Y. Wu and Z. Zhang, *J. Mater. Chem.*, 2012, **22**, 15198-15205.

11 D. Yu, Y. Xue and L. Dai, *J. Phys. Chem. Lett.* 2012, **3**, 2863−2870.

12 Y. Li, Z. Zhou, G. Yu, W. Chen and Z. Chen, *J. Phys. Chem. C*, 2010, **114**, 6250–6254.

13 D. Yu, E. Nagelli, F. Du and L. Dai, *J. Phys. Chem. Lett.*, 2010, **1**, 2165–2173.

14 E. H. Song, Z. Wen and Q. Jiang, *J. Phys. Chem. C*, 2011, **115**, 3678–3683.

15 S. Lin, X. Ye, R. S. Johnson and H. Guo, *J. Phys. Chem. C*, 2013, **117**, 17319−17326.

16 P. Zhao, Y. Su, Y. Zhang, S.-J. Li and G. Chen, *Chem. Phys. Lett.*, 2011, **515**, 159–162.

17 C. Stampfl and M. Scheffler, *Phys. Rev. Lett.*, 1997, **78**, 1500-1503.

18 P. Sabatier, *Ber. Deutsch. Chem. Gesellschaft*., 1911, **44**, 1984-2001.

19 J. K. Nørskov, T. Bligaard, J. Rossmeisl and C. H. Christensen, *Nature Chem.*, 2009, **1**, 37-46.

20 J. K. Nørskov, F. Abild-Pedersen, F. Studt and T. Bligaard, *Proc. Nat. Aca. Sci.*, 2011, **108**, 937-943.

21 A. H. M. A. Wasey, S. Chakrabarty, G. P. Das and C. Majumder, *ACS Appl. Mater. Interfaces*, 2013, **5,** 10404–10408.

22 M. D. Segall, P. J. D. Lindan, M. J. Probert, C. J. Pickard, P. J. Hasnip, S. J. Clark and M. C. Payne, *J. Phys.: Condens. Matter*, 2002, **14**, 2717−2744.

23 Vanderbilt, D. *Phys. Rev. B*, 1990, **41**, 7892−7895.

24 J. P. Perdew, K. Burke and M. Ernzerhof, *Phys. Rev. Lett.*, 1996, **77**, 3865−3868.

25 A. Tkatchenko and M. Scheffler, *Phys. Rev. Lett.*, 2009, **102**, 073005.

26 G. Kresse and J. Furthmüller, *Comput. Mat. Sci.*, 1996, **6,** 15-50.

27 G. Kresse and J. Furthmüller, *Phys. Rev. B*, 1996, **54**, 11169-11186.

28 N. Govind, M. Petersen, G. Fitzgerald, D. King-Smith and J. Andzelm, *Comput. Mater. Sci.*, 2003, **28**, 250-258.

29 O. L. Krivanek, M. F. Chisholm, V. Nicolosi, T. J. Pennycook, G. J. Corbin, N. Dellby, M. F. Murfitt, C. S. Own, Z. S. Szilagyi1, M. P. Oxley, S. T. Pantelides and S. J. Pennycook, *Nature*, 2010, **464**, 571-574.

30 P. A. Denis, *Comp. Mater. Sci.*, 2013, **67**, 203-206.

31 J. Cho, R. Sarangi, J. Annaraj, S. Y. Kim, M. Kubo, T. Ogura, E. I. Solomon and W. Nam, *Nat. Chem.*, 2009, **1**, 568-572.

32 R. Thapa and N. Park, *J. Phys. Chem. Lett.*, 2012, **3**, 3065-3069.

33 P. Atkins and J. Paula, in *Atkins' Physical Chemistry,* W. H. Freeman and Company, New York, 8th edn., 2006, pp. 993-1001.

34 F. Li, J. Zhao and Z. Chen, *J. Phys. Chem. C*, 2012, **116**, 2507–2514.

35 Y. Tang, Z. Yang, X. Dai, D. Ma and Z. Fu, *J. Phys. Chem. C*, 2013, **117**, 5258−5268.

36 Y.-H. Lu, M. Zhou, C. Zhang and Y.-P. Feng, *J. Phys. Chem. C*, 2009, **113**, 20156-20160.

37 P. Zhang, X. F. Chen, J. S. Lian and Q. Jiang, *J. Phys. Chem. C*, 2012, **116**, 17572−17579.

38 J.-X. Zhao, Y. Chen and H.-G. Fu, *Theor. Chem. Acc.*, 2012, **131**, 1242(1) – 1242(11).

39 C. Huang, X. Ye, C. Chen, S. Lin and D. Xie, *Comp. Theor. Chem.*, 2013, **1011,** 5–10.

40 Z.-P. Liu, X.-Q. Gong, J. Kohanoff, C. Sanchez and P. Hu, *Phys. Rev. Lett.*, 2003, **91**, 266102(1) - 266102(4).

41 Y.-P. Xie and X.-G. Gong, *J. Chem. Phys.*, 2010, **132**, 244302(1)-244302(6).

42 D. Tang, Z. Chen, J. Hu, G. Sun, S. Lu and C. Hu, *Phys. Chem. Chem. Phys.*, 2012, **14**, 12829–12837.

43 S. Dobrin, *Phys. Chem. Chem. Phys.,* 2012, **14,** 12122–12129.

44 S. Liu, R. Maoz, G. Schmid and J. Sagiv, *Nano Lett.*, 2002, **2**, 1055-1060.

45 Z. P. Liu, P. Hu and A. Alavi, *J. Am. Chem. Soc*., 2002, **124,** 14770–14779.

46 T. Jiang, D. J. Mowbray, S. Dobrin, H. Falsig, B. Hvolbæk, T. Bligaard and J. K. Nørskov, *J. Phys. Chem. C*, 2009, **113**, 10548–10553.

47 H. Falsig, B. Hvolbæk, I. S. Kristensen, T. Jiang, T. Bligaard, C. H. Christensen and J. K. Nørskov, *Angew. Chem. Int. Ed*. 2008, **47**, 4835 –4839.

Table 1: Bond lengths, adsorbate-surface distance (D), adsorption energies of O_2 adsorbed on different surfaces and the post-adsorption Mulliken charges on the adsorption site (Q_s), each atom of the O_2 molecule (Q_o) and the dopant (Q_d)

Surface	Site	O_2 bond length (Å)	D (Å)	E_{ad}(eV)		Mulliken Charge (e)		
				PBE	**PBE+D**	**Q_s**	**Q_o**	**Q_d**
CBN	B	1.34	1.58	-1.77	-1.91	+0.87	-0.27	+0.48
2CBN	B	1.53	1.48	-3.93	-4.07	+0.87	-0.45	+0.48
OBN	B1	1.34	1.55	-2.92	-3.04	+0.91	-0.27	-0.64

Table 2: Bond lengths, adsorbate-surface distance (D), adsorption energies of CO adsorbed on different surfaces and the Mulliken charge on the adsorption site.

Surface	Site	CO bond length (Å)	D (Å)	E_{ad} (eV)		Mulliken charge (e)
				PBE	**PBE+D**	
CBN	B	1.16	2.98	-0.03	-0.14	+0.82
CBN	C	1.17	2.43	-0.15	-0.31	+0.340
2CBN	B	1.20	1.73	-0.08	-0.24	+0.650
2CBN	C	1.18	2.21	-0.28	-0.44	+0.310
OBN	B1	1.20	1.64	-1.20	-1.33	+0.670

Graphitic Materials						
catalyst	**CO bond (Å)**	**E_{ad} (CO)**	**O_2 bond(Å)**	**E_{ad} (O_2)**	**Mechanism**	**E_a (RDS)**
Cu/graphene[14]	1.15	-1.71	1.35	-2.67	LH followed by ER	0.25, 0.54
Fe anchored graphene oxide [34]	1.15	-1.53	1.39	-2.09	ER	0.6, 0.7
Pt/D-graphene (D = B, N, O, Si, S, and P)[35]	1.16 to 1.17	-1.7 to -2.67	1.31 to 1.36	-0.77 to-1.64	Both ER and LH	$0.41\text{-}0.77^{LH}$, 0.72 to 1.07^{ER}
Au embedded graphene[36]	1.15	-1.53	1.35	-1.34	LH followed by ER	0.31, 0.18
Fe/N/C catalysts[37]	1.17	-1.0 to -2.28	1.41	-0.98 to -3.43	LH followed by ER	0.03 - 1.53
Fe embedded graphene[12]	1.15	-1.38	1.39	-1.65	ER	0.58
Si embedded graphene [38]	1.16	-0.17	1.5	-1.18	LH followed by ER	0.48, 0.57
Catalysts based on hexagonal boron nitride						
Fe embedded h-BN[16]	1.15	-1.27	1.34	-1.83	ER	0.56, 0.61
Ruthenium/hBN[39]	1.17	-1.95	1.42	-2.43	ER, LH	0.42, 0.77
Metal doped hBN[15]	1.17	-0.84 to -2.29	1.35	-0.54 to -2.37	ER	0.52
h-BN/Ni111[21]	1.15	no interaction	1.51	-1.87	ER	spontaneous
C doped h-BN (This work)	***1.16***	***-0.14, -0.31***	***1.34***	***-1.91***	***ER***	***0.26***
O doped h-BN (This work)	***1.20***	***-1.33***	***1.34***	***-3.04, -1.73***	***ER, LH***	$\boldsymbol{0.16^{ER}, 1.55^{LH}}$
Metal based catalysts						
unsupported Au[40]	--	-1.69	--	-0.07	LH	>2
TiO_2 supported gold[40]	--	-1.24 to-1.38	--	-0.6 to -0.86	ER	0.1 to 0.17
Au_{55} nanocluster[41]	--	-0.5 to -0.71	--	-0.08, -0.1	LH	0.56
Ag_{55} nanocluster[42]	--	-0.39 to -0.42	1.31 to 1.41	-0.28 to -0.34	LH, ER	0.53^{ER}, 0.75^{LH}
Au_{55} nanocluster[4]	1.15	-1.65	1.26	-0.47	LH	0.79
Pt_{55} nanocluster[43]	-	-	-	-	LH	1.32 to 1.49
Au_{55} nanocluster (This work)	***1.16***	***-0.77***	***1.26***	***-0.49***	***LH***	***0.76***
Pt_{55} nanocluster (This work)	***1.17***	***-1.51***	***1.38***	***-1.79***	***LH***	***0.60***

Table 3: Comparison of bond lengths and adsorption energies of reactants, CO oxidation mechanism and activation barrier of the rate determining step during CO oxidation for different classes of catalysts.

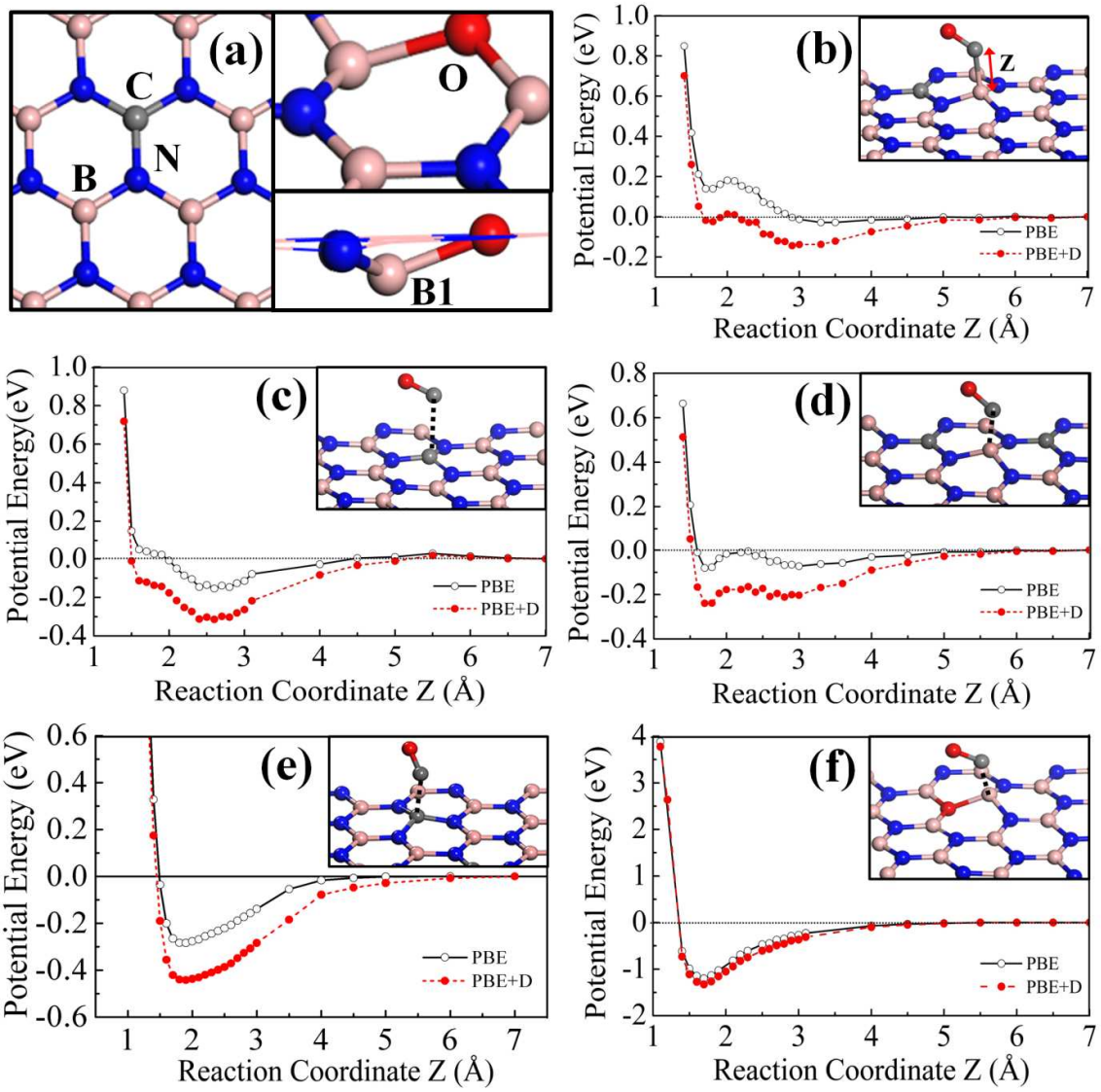

Fig. 1. a) optimized geometries of C and O doped hBN sheet. The pink, blue, grey and red balls represent the boron, nitrogen, carbon and oxygen atoms respectively. B1 indicates the distorted boron atom. (b) constraint potential energy curves of CO approaching (b) B site of CBN, (c) C site of CBN (d) B site of 2CBN (e) C site of 2CBN and (f) B site of OBN. The reaction coordinate (Z) is chosen to be the vertical distance of CO from each of the surfaces. The points are connected by lines to guide the eye.

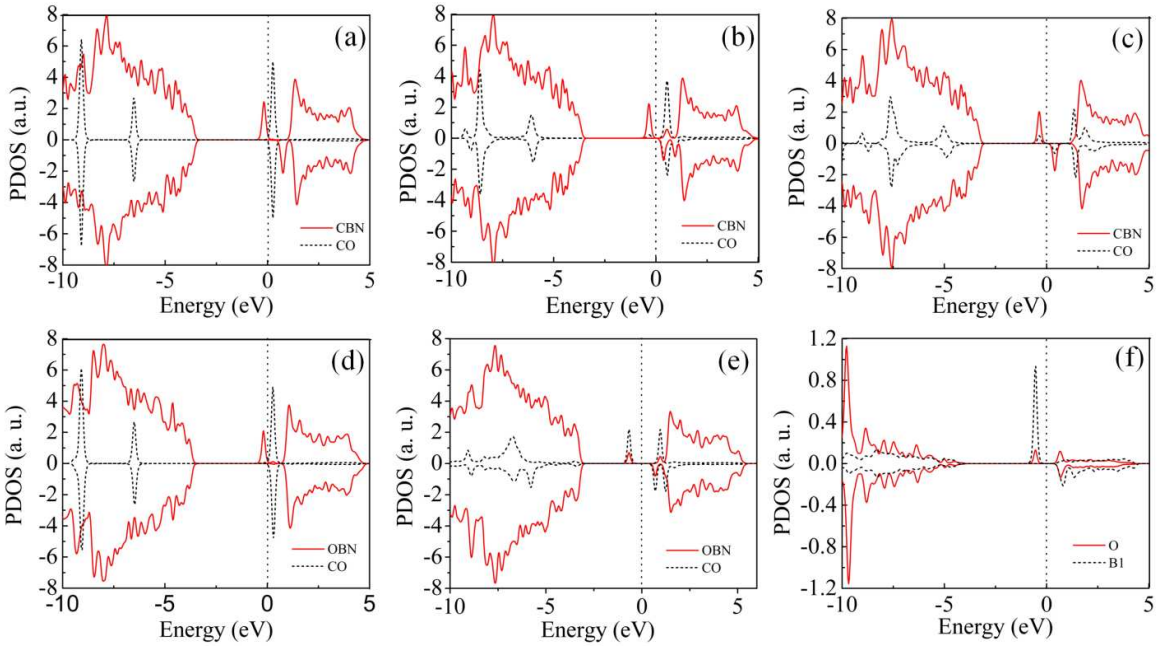

Fig. 2. Partial density of states of CO molecule and the catalyst (a) before adsorption of CO molecule on CBN surface (b) after adsorption on B site of CBN, (c) after adsorption on C site of CBN, (d) before adsorption on OBN, (e) after adsorption on B site of OBN, (f) PDOS of the active boron site (B1) and the O dopant site of OBN. The red solid line represents the PDOS of the doped surface and the black dashed line indicates the PDOS of CO molecule. The B1 atom is shown the Fig. 1 (a).

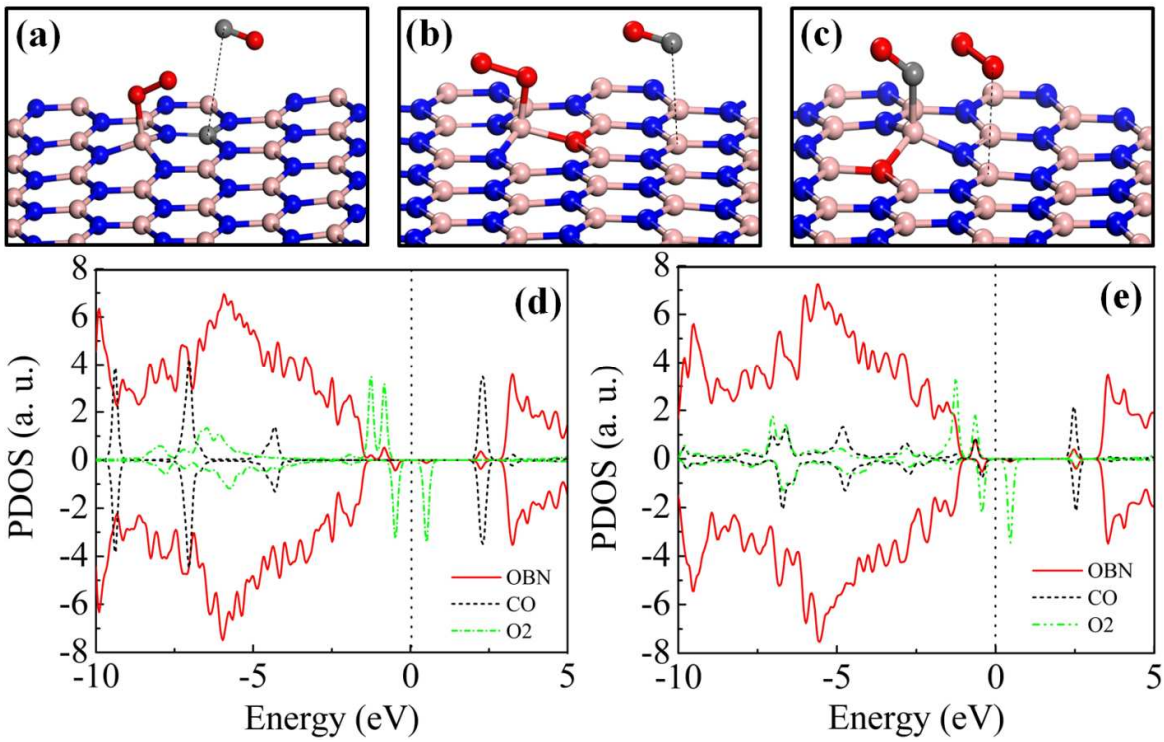

Fig. 3. Demonstrate the O_2 and CO co-adsorption behavior, (a) CO on CBN pre-adsorbed with O_2. (b) and (d) CO on OBN pre-adsorbed with O_2. (c) and (e) O_2 on OBN pre-adsorbed with CO. The red solid line denotes the PDOS of OBN surface, the dashed black line represents the CO molecule and the green dot-dashed line represents the PDOS of O_2 molecule.

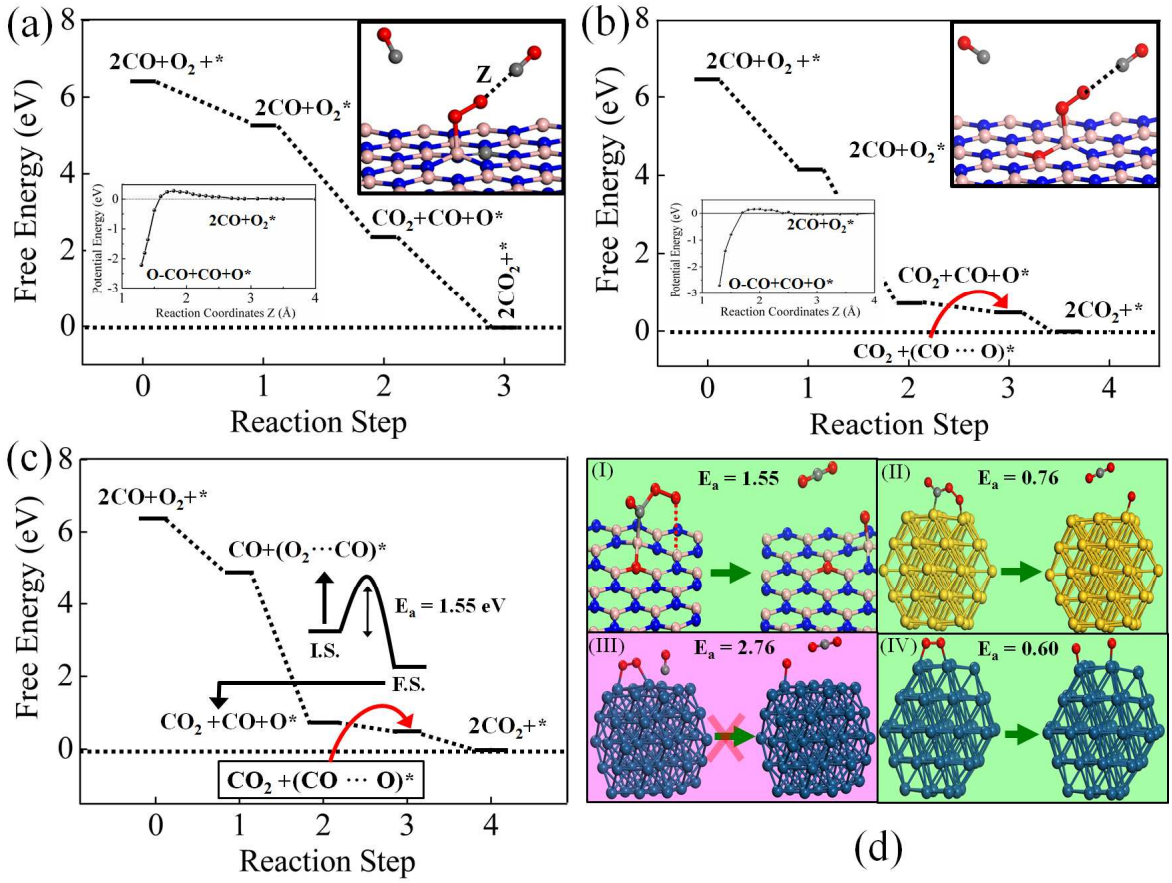

Fig. 4. Free energy pathways of CO oxidation on (a) CBN surface via ER mechanism. The upper right inset shows the structure used to obtain the constrained potential energy curve. The reaction coordinate (Z) is taken to be the distance of the CO molecule from the adsorbed O_2 molecule. The lower left inset shows the constraint PE curve employed to calculate the energy barrier for desorption of first CO. (b) OBN surface via ER mechanism, the insets are with similar consideration as in Fig. 1 (a). (c) OBN surface via LH mechanism. (d) RDS and calculated activation barriers of CO oxidation following LH mechanism on (I) OBN surface (II) Au_{55} cluster (III) Pt_{55} cluster with CO reacting with molecular O_2 (IV) O_2 dissociation. The yellow and dark blue spheres represent gold and platinum atoms. The other colored spheres represent the same atoms as depicted in Fig. 1. The initial state and final states are denoted as I.S. and F.S. The * sign indicates the catalytic surface, and the adsorbed state of molecules and atoms are denoted with a * sign. The dotted lines are to guide the eye.

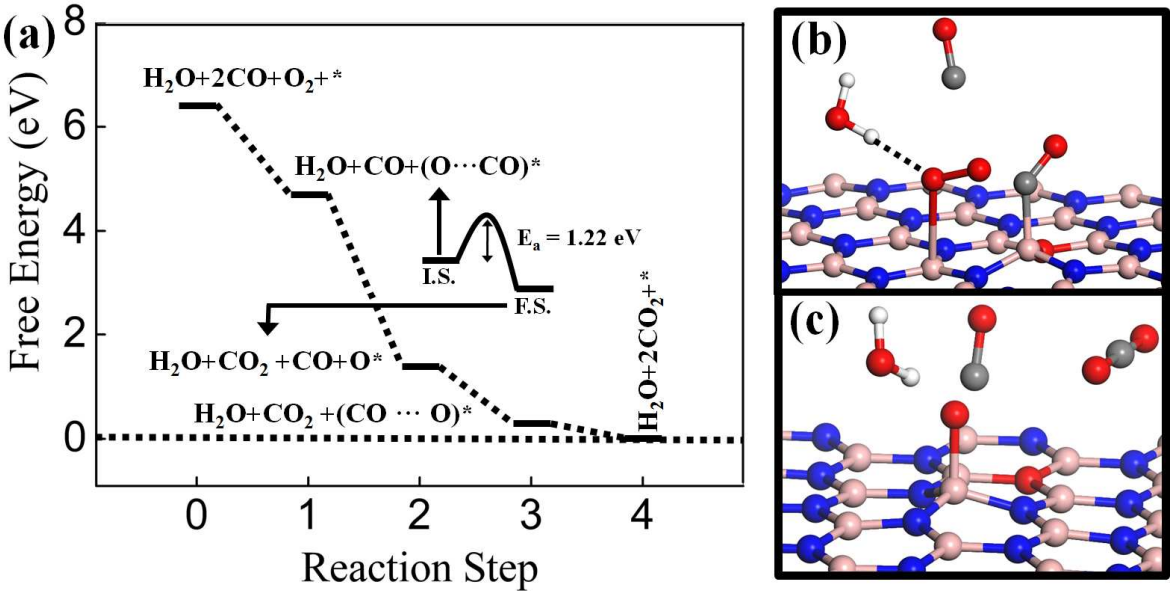

Fig. 5. (a) Free energy pathways for water - enhanced CO oxidation via LH mechanism on the OBN surface. (b) optimized structure of IS for RDS of Fig. 5a (c) optimized structure of FS for RDS of Fig. 5a. The symbols are same convention as in Fig. 4.